

## 基于压电振动能量俘获的弯曲结构损伤监测研究

赵翔, 李思谊, 李映辉

## THE RESEARCH ON DAMAGE DETECTION OF CURVED BEAM BASED ON PIEZOELECTRIC VIBRATION ENERGY HARVESTER

Zhao Xiang, Li Siyi, and Li Yinghui

在线阅读 View online: <https://doi.org/10.6052/0459-1879-21-452>

### 您可能感兴趣的其他文章

#### Articles you may be interested in

#### 曲梁压电俘能器强迫振动的格林函数解

CLOSED-FORM SOLUTIONS FOR FORCED VIBRATIONS OF CURVED PIEZOELECTRIC ENERGY HARVESTERS BY MEANS OF GREEN'S FUNCTIONS

力学学报. 2019, 51(4): 1170-1179

#### 附磁压电悬臂梁流致振动俘能特性分析

ENERGY HARVESTING ANALYSIS OF A PIEZOELECTRIC CANTILEVER BEAM WITH MAGNETS FOR FLOW-INDUCED VIBRATION

力学学报. 2019, 51(4): 1148-1155

#### 主动控制压电旋转悬臂梁的参数振动稳定性分析

STABILITY ANALYSIS ON PARAMETRIC VIBRATION OF PIEZOELECTRIC ROTATING CANTILEVER BEAM WITH ACTIVE CONTROL

力学学报. 2019, 51(6): 1872-1881



关注微信公众号, 获得更多资讯信息

# 基于压电振动能量俘获的弯曲结构损伤监测研究<sup>1)</sup>

赵 翔<sup>\*,2)</sup> 李思谊<sup>\*</sup> 李映辉<sup>†</sup>

<sup>\*</sup>(西南石油大学土木工程与测绘学院工程安全评估与防护研究院, 成都 610500)

<sup>†</sup>(西南交通大学力学与工程学院, 成都 610500)

**摘要** 建立了含裂纹损伤的曲梁压电能量俘获系统在强迫振动下的动力学模型. 基于 Prescott 型压电曲梁力电耦合振动方程的解析解和裂纹截面处的连续性条件, 求解了含裂纹损伤的压电曲梁的格林函数. 根据线性叠加原理, 对含裂纹的力电耦合模型的系统方程解耦, 得到强迫振动下含裂纹损伤的曲梁压电俘能器的输出电压. 在得到模型的强迫振动解析解后, 提出逆方法检测结构中的裂纹损伤, 这一检测方法适用于处于振动状态下的结构. 在数值计算中, 令裂纹深度为零, 通过对比本文的解析解与现有文献中的解析解, 验证了本文解的有效性. 分别分析了含裂纹损伤的压电曲梁的电压响应与裂纹深度、裂纹位置、材料的几何参数以及阻尼之间的关系. 研究表明: 裂纹的存在对曲梁式压电俘能器的影响比直梁式更加复杂; 裂纹出现时, 损伤曲梁在健康曲梁的一阶频率值处一定会出现波动并被激励出二阶频率, 此时的二阶频率是开路中健康压电曲梁的一阶频率值; 通过对电压响应的检测可以确定的损伤裂纹的深度和在结构中出现的位置范围; 利用振动问题的解来检测压电曲梁的健康状况是可行且准确的.

**关键词** 压电俘能器, 压电裂纹曲梁, 力电耦合, 损伤检测, 格林函数

中图分类号: O327 文献标识码: A doi: 10.6052/0459-1879-21-452

## THE RESEARCH ON DAMAGE DETECTION OF CURVED BEAM BASED ON PIEZOELECTRIC VIBRATION ENERGY HARVESTER<sup>1)</sup>

Zhao Xiang<sup>\*,2)</sup> Li Siyi<sup>\*</sup> Li Yinghui<sup>†</sup>

<sup>\*</sup>(School of Civil Engineering and Geomatics, Research Institute of Engineering Safety Assessment and Protection, Southwest Petroleum University, Chengdu 610500, China)

<sup>†</sup>(School of Mechanics and Engineering, Southwest Jiaotong University, Chengdu 610500, China)

**Abstract** This paper established dynamic model of forced vibration of the curved piezoelectric energy harvesters with cracks. The Green's function of piezoelectric curved beam with cracks is obtained based on analytical solutions of vibration equation of the electromechanical coupled Prescott models and continuity conditions at crack sections. The system equation of the electromechanical coupled model with cracks is decoupled and the output voltage of the forced vibration of the damaged curved piezoelectric energy harvester under forced vibration is acquired by the linear superposition principle. The damaged conditions of the piezoelectric curved beam can be detected by inverse method, which is proposed in this paper and suitable for the structure in vibration. In the numerical simulations, the analytical solutions of damaged piezoelectric curved beam that have zero crack depth are compared with results in the previous

2021-09-06 收稿, 2021-10-19 录用, 2021-10-20 网络版发表.

1) 国家自然科学基金资助项目 (12072301, 11372257).

2) 赵翔, 副教授, 主要研究方向: 动力学与控制. E-mail: zhaoxiang\_swpu@126.com

引用格式: 赵翔, 李思谊, 李映辉. 基于压电振动能量俘获的弯曲结构损伤监测研究. 力学学报, 2021, 53(11): 3035-3044

Zhao Xiang, Li Siyi, Li Yinghui. The research on damage detection of curved beam based on piezoelectric vibration energy harvester. *Chinese Journal of Theoretical and Applied Mechanics*, 2021, 53(11): 3035-3044

references. The validity of solutions in this paper is verified. The influence of the crack depth, crack location, material geometric parameters and damping on frequency responses of the voltage is investigated separately. The results show that the effect of cracks on the curved piezoelectric energy harvester is more complicated than that of the straight beam model. The voltage response of damaged piezoelectric curved beam is proportionally decrease at the first order frequency that is the first order frequency of healthy curved beam. And the damaged piezoelectric curved beam is excited out the second-order frequency, which is the first order frequency value of healthy piezoelectric curved beam in an short-circuit. The depth of cracks and the range of cracked positions in the piezoelectric curved beam can be determined by monitoring the change of voltage response, which verifies the feasibility of the inverse method. It is feasible and accurate to use the solution of vibration problem to detect the health condition of damaged piezoelectric curved beams.

**Key words** piezoelectric energy harvester, cracked-piezoelectric curved beam, electromechanical, damage detection, Green's function

## 引言

近年来,压电材料因其具有能实现电能和机械能互相转换的特性,在工程结构中日益受到重视<sup>[1-2]</sup>,被广泛应用于结构的形状控制、振动和噪声控制、损伤检测等领域<sup>[3-4]</sup>。从机械振动中提取能量的特性极大满足了传感器自给供电的经济需求与生态需求,因此压电材料广泛应用于俘能器中<sup>[5-6]</sup>。到目前为止,最常用的压电俘能器采用悬臂梁式,通常是由一个结构层和压电材料(如压电陶瓷 PZT、压电复合材料 PVDF)层组成<sup>[7]</sup>。学者们对直梁压电振动能量俘获系统进行了大量且详细的研究。Erturk 和 Inman<sup>[8-9]</sup>在 Euler-Bernoulli 梁假设下,研究了在基座横向运动时悬臂式压电俘能器横向振动的精确解析解。另外考虑到常用的单自由度谐波激励对预测悬臂梁的运动可能会产生不准确的结果,推导了修正因子以改进单自由度横向和纵向振动激励模型。Zhao 等<sup>[10]</sup>应用格林函数法对悬臂式 Timoshenko 直梁压电俘能器进行了动力学分析,得到了强迫振动的解析解,探究了各类因素对电压响应的影响。Zhou 和 Lei<sup>[11]</sup>研究了非对称三稳态压电俘能器的非线性动力学特性,以提高不同激励下的能量收集性能。Huang 等<sup>[12]</sup>对电阻-电感谐振电路非线性能量采集器的稳态响应机制进行了理论研究。Fang 等<sup>[13]</sup>根据哈密顿原理提出了利用离心软化效果分析旋转冲击能量俘获的理论模型。

而曲梁形式的压电俘能器的优点在于可用于多方向振动能量收集<sup>[14]</sup>,在微型电子系统以及复杂边界的工程结构中应用广泛<sup>[15]</sup>。王剑等<sup>[16]</sup>构建了空间压电曲梁单元形状控制模型并得到了结构的最优形状控制电压。周勇等<sup>[17]</sup>提出了一种基于面内驱动的

层合压电悬臂曲梁形式微位移驱动结构,忽略方程中曲率半径的影响获得了该曲梁在外荷载作用下控制方程的解析解。丁维高和谢进<sup>[18]</sup>利用哈密顿原理,研究了在水平与数值方向简谐振动激励的作用下压电曲梁俘能器的机电耦合的解析解。Kathpalia 等<sup>[19]</sup>建立了采用智能陶瓷压电材料的弯曲式压电传感器的分析模型,并获得了封闭式机电频率响应方程。Chen 等<sup>[20]</sup>采用数值方法分析了具有弹性约束的功能梯度压电曲梁的自由振动特性和瞬时响应。Tabatabaei-Nejhad 等<sup>[21]</sup>研究了嵌入压电层的层压曲梁的平面外振动特性,考虑了扭转和弯曲变形造成的剪切变形和旋转惯性效应。何燕丽和赵翔<sup>[22]</sup>利用格林函数法求解 Prescott 型曲梁俘能器强迫振动的响应。

曲梁结构如今广泛地应用于各种领域的工程结构中,在外荷载激励下难免造成损伤产生裂纹,从而严重影响材料结构的整体性能和使用寿命<sup>[23-24]</sup>。对损伤曲梁的振动特性研究也一直是国内外研究的热点<sup>[24-27]</sup>。为识别结构中的损伤发展了许多检测方法,分别有超声波法、电涡流法、磁粉法和红外识别法<sup>[28]</sup>,以及基于结构振动特性的损伤识别法,后者具有明显的非破坏性,方便、快速、便宜的优点被广泛采用<sup>[28]</sup>。另外,还有基于压电效应的主动感应法对结构的健康监测和损伤检测方法。孙威等<sup>[29]</sup>利用智能压电传感器对混凝土构件的裂缝损伤发展状况进行监测,探索一种基于压电波动法的裂缝损伤监测方法。Hou 等<sup>[30]</sup>将压电智能材料和压电陶瓷材料应用于传感器,对地震力作用下的混凝土结构整体剪切应力进行监测研究。Markovic 等<sup>[31]</sup>建立了使用压电智能传感器的主动监测系统和损坏检测的有效有限元模型,对基于压电波动法的埋入式压电陶瓷混凝土

梁损伤识别系统进行模拟分析. 由此, 本文提出可以采用逆方法, 即通过振动引起的压电俘能器的信号响应变化分析曲梁的振动问题, 从而对结构进行损伤监测.

目前已经有不少学者对裂纹曲梁的振动问题和曲梁式压电俘能器进行了研究, 但是有关损伤曲梁式压电俘能器强迫振动问题的研究较少. 在上文已经阐述了裂纹存在给结构带来的负面影响, 因此对含裂纹损伤的曲梁压电俘能器的研究是有实际意义的. 本文不仅研究其强迫振动问题, 还采用逆方法, 即利用损伤曲梁振动时的俘能器电压响应变化, 提出了一种监测结构损伤的方法.

本文建立了含裂纹损伤的曲梁压电俘能器的机电耦合模型, 得到其强迫振动的解析解并基于压电俘能器的响应监测曲梁结构的损伤情况. 基于文献 [22] 中 Prescott 型曲梁压电俘能器的解析解, 引入局部刚度模型描述裂纹损伤截面的力学特性, 应用格林数法和传递矩阵法推导含多裂纹曲梁压电俘能器强迫振动下的解析解. 根据线性系统叠加原理, 对力电耦合系统解耦, 推导了该裂纹损伤模型的输出电压的解析式. 数值模拟了压电俘能器在曲梁结构处于振动状态下的响应信号, 提出了对结构进行损伤监测的方法, 以期为曲梁式压电俘能器的振动研究以及损伤结构的监测和优化设计提供理论参考.

### 1 损伤曲梁压电俘能器的机电耦合模型

建立如图 1 所示的含裂纹损伤的悬臂式曲梁压电俘能器模型. 俘能器中的压电层材料比结构层材料的柔性好, 因此结构层上更容易产生裂纹. 如图 1(a) 所示, 该模型结构层上存在  $n$  个开口裂纹, 假设受到外力作用时, 裂纹截面处的局部刚度发生变化, 曲梁的挠度出现不连续性, 曲梁的未损伤部分没有受到影响[32]. 因此, 在裂纹损伤截面处建立局部柔度模型用来描述截面的力学特性, 将裂纹处视为一个刚度为  $K_{eq}$  的等效无质量扭转弹簧, 该弹簧连接着相邻的两个完整部分, 可表示为

$$K_{eq} = \frac{EI}{h_s} \frac{1}{\bar{C}_W} \quad (1)$$

式中  $EI$  为压电曲梁的有效刚度,  $h_s$  是结构层曲梁的高度,  $\bar{C}_W$  局部柔度的无量纲常数, 在本模型中采用

$$\bar{C}_W = 5.346h'^2 (1.86 - 3.95h' + 16.375h'^2 - 37.226h'^3 + 76.81h'^4 - 126.9h'^5 + 172h'^6 - 143.97h'^7 + 66.56h'^8) \quad (2)$$

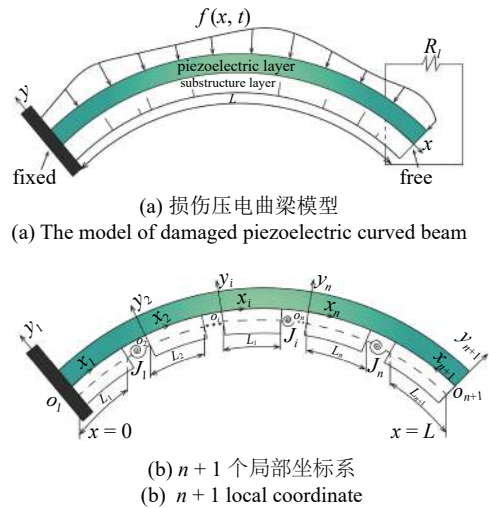


图 1 损伤曲梁压电俘能器模型

Fig. 1 The model of curved piezoelectric energy harvester with  $n$  cracks

式中  $h' = h_c/h_s$  是裂纹深度与曲梁高度的比值.

如图 1(b) 所示, 压电曲梁被  $n$  个裂纹分成  $n+1$  段完整部分, 每段长度为  $L_i (i = 1, 2, \dots, n+1)$  并且由一个等效无质量扭转弹簧连接. 为了得到裂纹压电曲梁的格林函数, 需要分别研究每段的变形情况. 因此, 建立  $n+1$  个局部坐标系  $o_i x_i y_i (i = 1, 2, \dots, n+1)$  [33] 表示出每段的格林函数后, 转换局部坐标为全局坐标即  $x_1 = x, x_i = x - \sum_{j=1}^{i-1} L_j (i = 2, 3, \dots, n), x_{n+1} = L = x$ , 即可得到压电曲梁的格林函数.

已知文献 [22] 中建立的 Prescott 曲梁模型, 没有考虑曲梁轴向力以及轴向惯性项, 仅考虑了曲梁的径向位移. 因此曲梁压电俘能器的振动控制方程是一个四阶偏微分方程, 引用文献 [22] 中的格林函数, 该格林函数是强迫振动下的压电曲梁径向位移  $W(x)$  的解

$$\left. \begin{aligned} G_1(x; x_0) &= H(x-x_0)\phi_{11}(x-x_0) + \phi_2(x)W_1(x) + \\ &\quad \phi_3(x)W_1'(x) + \phi_4(x)W_1''(x) + \phi_5(x)W_1'''(x) \\ G_2(x; x_0) &= \bar{V}H(x-x_0)\phi_{12}(x-x_0) + \phi_2(x)W_2(x) + \\ &\quad \phi_3(x)W_2'(x) + \phi_4(x)W_2''(0) + \phi_5(x)W_2'''(0) \\ G_3(x; x_0) &= \bar{V}H(x-x_0)\phi_{13}(x-x_0) + \phi_2(x)W_3(x) + \\ &\quad \phi_3(x)W_3'(x) + \phi_4(x)W_3''(0) + \phi_5(x)W_3'''(0) \end{aligned} \right\} n \quad (3)$$

式中  $x_0$  表示单位力作用的位置,  $W'_i, W''_i, W'''_i$  是径向位移  $W_i (i = 1, 2, 3)$  的各阶导数,  $\bar{V}$  表示压电俘能器的电压.  $G_1(x, x_0)$  表示由外力引起的位移解,  $G_2(x, x_0)$ ,

$G_3(x, x_0)$  是由电耦合效应引起的位移解, 且有

$$\left. \begin{aligned} \phi_{11}(x) &= \sum_{i=1}^4 A_i(x)(b_1 s_i^2 - b_2) \\ \phi_{12}(x) &= \sum_{i=1}^4 A_i(x)(-b_3 s_i) \\ \phi_{13}(x) &= \sum_{i=1}^4 A_i(x)(c s_i^{-1}) \\ \phi_2(x) &= \sum_{i=1}^4 A_i(x)(s_i^3 + a_1 s_i) \\ \phi_3(x) &= \sum_{i=1}^4 A_i(x)(s_i^2 + a_1) \\ \phi_4(x) &= \sum_{i=1}^4 A_i(x) s_i \\ \phi_5(x) &= \sum_{i=1}^4 A_i(x) \end{aligned} \right\} \quad (4)$$

$$\left. \begin{aligned} A_1(x) &= \frac{e^{s_1 x}}{(s_1 - s_2)(s_1 - s_3)(s_1 - s_4)} \\ A_2(x) &= \frac{e^{s_2 x}}{(s_2 - s_1)(s_2 - s_3)(s_2 - s_4)} \\ A_3(x) &= \frac{e^{s_3 x}}{(s_3 - s_1)(s_3 - s_2)(s_3 - s_4)} \\ A_4(x) &= \frac{e^{s_4 x}}{(s_4 - s_1)(s_4 - s_2)(s_4 - s_3)} \end{aligned} \right\}$$

式 (4) 和式 (5) 中

$$\left. \begin{aligned} a_1 &= \frac{1}{R^2} + \frac{\gamma \Omega^2}{EI} + \frac{i \Omega c_1 - \mu \Omega^2}{EA} \\ a_2 &= \frac{(i \Omega c_1 - \mu \Omega^2) \gamma \Omega^2}{EIEA} + \frac{\gamma \Omega^2}{EIR^2} \\ b_1 &= \frac{1}{EA} \\ b_2 &= \frac{\gamma \Omega^2}{EIEA} \\ b_3 &= \frac{\vartheta_2}{EAR} + \frac{\vartheta_1}{EI} \\ c &= -\frac{\gamma \Omega^2 \vartheta_2}{EIEAR} \end{aligned} \right\} \quad (6)$$

且  $s_i (i = 1, 2, 3, 4)$  是下列代数方程的根

$$s^4 + a_1 s^2 + a_2 = (s_1 - s_1)(s_1 - s_2)(s_1 - s_3)(s_1 - s_4) \quad (7)$$

式 (6) 中,  $R$  是曲梁的半径,  $\mu$  和  $\gamma$  表示单位长度曲梁的质量和转动惯量,  $c_1$  表示阻尼系数,  $A$  表示截面面积.  $\vartheta_1$  和  $\vartheta_2$  是力电耦合系数, 具体表达式见文献 [22].

在本文的后续推导中需要用到轴向位移, 根据曲梁控制方程 [22] 可推出轴向位移  $V(x)$

$$\begin{aligned} V(x) &= d_1 W''''(x) + d_2 W'(x) + d_1 F(x) + \\ & d_3 \bar{V}[\delta(x - x_1) - (x - x_2)] + d_4 \bar{V}[\delta(x - x_1) - (x - x_2)] \end{aligned} \quad (8)$$

式中

$$\left. \begin{aligned} d_1 &= \frac{EIR}{\gamma \Omega^2} \\ d_2 &= \frac{ic_1 EIR}{\gamma \Omega EA} - \frac{\mu EIR}{\gamma EA} - \frac{EI}{\gamma \Omega^2 R} + R \\ d_3 &= \vartheta_1 \\ d_4 &= \frac{\vartheta_2 EI}{EAR} \end{aligned} \right\} \quad (9)$$

根据式 (3) ~ 式 (9) 得到由外荷载引起的轴向位移的格林函数

$$\begin{aligned} V_1(x; x_0) &= H(x - x_0) \bar{\phi}_{11}(x - x_0) + \bar{\phi}_2(x) W_1(x) + \\ & \bar{\phi}_3(x) W_1'(x) + \bar{\phi}_4(x) W_1''(x) + \bar{\phi}_5(x) W_1'''(x) \end{aligned} \quad (10)$$

式中,  $\bar{\phi}_m = (d_1 s_i^3 + d_2 s_i) \phi_m (m = 2, 3, 4, 5, 11)$ . 因此, 局部坐标系下的格林函数为

$$\left. \begin{aligned} W_{1i}(x_i; x_{i0}) &= \bar{G}_{1i}(x_i; x_{i0}) = \\ & H(x_i - x_{i0}) \phi_{11}(x_i - x_{i0}) + \phi_2(x_i) W_{1i}(x) + \\ & \phi_3(x_i) W_{1i}'(x) + \phi_4(x_i) W_{1i}''(x) + \phi_5(x_i) W_{1i}'''(x) \\ V_{1i}(x_i; x_{i0}) &= H(x_i - x_{i0}) \bar{\phi}_{11}(x_i - x_{i0}) + \bar{\phi}_2(x_i) W_{1i}(x) + \\ & \bar{\phi}_3(x_i) W_{1i}'(x) + \bar{\phi}_4(x_i) W_{1i}''(x) + \bar{\phi}_5(x_i) W_{1i}'''(x) \end{aligned} \right\} \quad (11)$$

式中,  $W_{1i}(x), W_{1i}'(x), W_{1i}''(x), W_{1i}'''(x)$  是待解的未知常数. 为了求解系统中的  $4n + 4$  个未知常数, 在压电曲梁的裂纹截面处建立各状态矢量 (横向位移、弯矩、剪力和转角位移) 之间传递关系, 应用传递矩阵法求解局部格林函数.

在第  $i (i = 1, 2, \dots, n - 1)$  个裂纹位置处和在第  $n$  个裂纹位置处各状态矢量的传递关系 [34] 如式 (12) 和式 (13) 所示, 曲梁的轴向位移、弯矩相等, 剪力大小相等但在第  $n$  处方向相反, 截面转角始终不连续

$$\left. \begin{aligned}
 &W_{1i} \Big|_{x_i=L_i^-} = W_{1i+1} \Big|_{x_{i+1}=0^+} \\
 &\frac{\partial^2 W_{1i}}{\partial x_i^2} - \frac{1}{R} \frac{\partial V_{1i}}{\partial x_i} \Big|_{x_i=L_i^-} = \frac{\partial^2 W_{1i+1}}{\partial x_{i+1}^2} - \frac{1}{R} \frac{\partial V_{1i+1}}{\partial x_{i+1}} \Big|_{x_{i+1}=0^+} \\
 &-\left( \frac{\partial^3 W_{1i}}{\partial x_i^3} - \frac{1}{R} \frac{\partial^2 V_{1i}}{\partial x_i^2} \right) \Big|_{x_i=L_i^-} = -\left( \frac{\partial^3 W_{1i+1}}{\partial x_{i+1}^3} - \frac{1}{R} \frac{\partial^2 V_{1i+1}}{\partial x_{i+1}^2} \right) \Big|_{x_{i+1}=0^+} \\
 &\frac{1}{R} \frac{\partial^2 V_{1i+1}}{\partial x_{i+1}^2} \Big|_{x_{i+1}=0^+} \theta_{1i} \Big|_{x_i=L_i^-} = -J_i EI \left( \frac{\partial^2 W_{1i+1}}{\partial x_{i+1}^2} - \frac{1}{R} \frac{\partial V_{1i+1}}{\partial x_{i+1}} \right) \Big|_{x_{i+1}=0^+} + \theta_{i+1} \Big|_{x_{i+1}=0^+}
 \end{aligned} \right\} \begin{aligned}
 &\begin{bmatrix} \phi_2(L_i) & \phi_3(L_i) & \phi_4(L_i) & \phi_5(L_i) \\ \varphi'_2(L_i) & \varphi'_3(L_i) & \varphi'_4(L_i) & \varphi'_5(L_i) \\ -\varphi''_2(L_i) & -\varphi''_3(L_i) & -\varphi''_4(L_i) & -\varphi''_5(L_i) \\ \varphi_2(L_i) & \varphi_3(L_i) & \varphi_4(L_i) & \varphi_5(L_i) \end{bmatrix} \\
 &T_{2i} = \begin{bmatrix} \Phi(0) \\ \varphi'(0) \\ -\varphi''(0) \\ \bar{\psi}(0) \end{bmatrix} =
 \end{aligned} \tag{12}$$

$$\left. \begin{aligned}
 &W_{1n} \Big|_{x_n=L_n^-} = W_{1n+1} \Big|_{x_{n+1}=L_{n+1}^-} \\
 &\frac{\partial^2 W_{1n}}{\partial x_n^2} - \frac{1}{R} \frac{\partial V_{1n}}{\partial x_n} \Big|_{x_n=L_n^-} = \frac{\partial^2 W_{1n+1}}{\partial x_{n+1}^2} - \frac{1}{R} \frac{\partial V_{1n+1}}{\partial x_{n+1}} \Big|_{x_{n+1}=L_{n+1}^-} \\
 &-\left( \frac{\partial^3 W_{1n}}{\partial x_n^3} - \frac{1}{R} \frac{\partial^2 V_{1n}}{\partial x_n^2} \right) \Big|_{x_n=L_n^-} = \frac{\partial^3 W_{1n+1}}{\partial x_{n+1}^3} - \frac{1}{R} \frac{\partial^2 V_{1n+1}}{\partial x_{n+1}^2} \Big|_{x_{n+1}=L_{n+1}^-} \\
 &\frac{1}{R} \frac{\partial^2 V_{1n+1}}{\partial x_{n+1}^2} \Big|_{x_{n+1}=L_{n+1}^-} \theta_{1n} \Big|_{x_n=L_n^-} = -J_n \left( \frac{\partial^2 W_{1n+1}}{\partial x_{n+1}^2} - \frac{1}{R} \frac{\partial V_{1n+1}}{\partial x_{n+1}} \right) \Big|_{x_{n+1}=L_{n+1}^-} - \theta_{1n+1} \Big|_{x_{n+1}=L_{n+1}^-}
 \end{aligned} \right\} \begin{aligned}
 &\begin{bmatrix} \phi_2(0) & \phi_3(0) & \phi_4(0) & \phi_5(0) \\ \varphi'_2(0) & \varphi'_3(0) & \varphi'_4(0) & \varphi'_5(0) \\ -\varphi''_2(0) & -\varphi''_3(0) & -\varphi''_4(0) & -\varphi''_5(0) \\ \bar{\psi}_{2i}(0) & \bar{\psi}_{3i}(0) & \bar{\psi}_{4i}(0) & \bar{\psi}_{5i}(0) \end{bmatrix} \\
 &K_i = H(-x_{i0}) \begin{bmatrix} \phi_{11}(-x_{i0}) \\ \varphi'_{11}(-x_{i0}) \\ -\varphi''_{11}(-x_{i0}) \\ \bar{\psi}_{1i}(-x_{i0}) \end{bmatrix} - \\
 &H(L_i - x_{i0}) \begin{bmatrix} \phi_{11}(L_i - x_{i0}) \\ \varphi'_{11}(L_i - x_{i0}) \\ -\varphi''_{11}(L_i - x_{i0}) \\ \varphi_{1i}(L_i - x_{i0}) \end{bmatrix}
 \end{aligned} \tag{13}$$

式中,  $\theta_{1m} = \frac{\partial W_{1m}}{\partial x} + \frac{1}{R} V_{1m} (m = 1, 2, \dots, n)$  表示截面转角;  $J_i$  和  $J_n$  表示第  $i$  处和第  $n$  处的等效扭转弹簧的局部柔度, 是刚度  $K_{eq}$  的倒数.

将局部格林函数式 (11) 带入传递关系式 (12) 和式 (13) 中可得到两个矩阵形式的传递方程

$$T_{1i}U_i = K_i + T_{2i}U_{i+1} \tag{14a}$$

$$T_{1n}U_n = K_n + T_{2n}U_{n+1} \tag{14b}$$

式中

$$U_i = [ W_{1i}(x) \quad W_{1i}'(x) \quad W_{1i}''(x) \quad W_{1i}'''(x) ]^T$$

$$T_{1i} = \begin{bmatrix} \Phi(L_i) \\ \varphi'(L_i) \\ -\varphi''(L_i) \\ \varphi(L_i) \end{bmatrix} =$$

$$U_n = [ W_{1n}(x) \quad W_{1n}'(x) \quad W_{1n}''(x) \quad W_{1n}'''(x) ]^T$$

$$T_{1n} = \begin{bmatrix} \Phi(L_n) \\ \varphi'(L_n) \\ -\varphi''(L_n) \\ \varphi(L_n) \end{bmatrix} =$$

$$\begin{bmatrix} \phi_2(L_n) & \phi_3(L_n) & \phi_4(L_n) & \phi_5(L_n) \\ \varphi'_2(L_n) & \varphi'_3(L_n) & \varphi'_4(L_n) & \varphi'_5(L_n) \\ -\varphi''_2(L_n) & -\varphi''_3(L_n) & -\varphi''_4(L_n) & -\varphi''_5(L_n) \\ \varphi_2(L_n) & \varphi_3(L_n) & \varphi_4(L_n) & \varphi_5(L_n) \end{bmatrix}$$

(15)

$$T_{2n} = \begin{bmatrix} \Phi(L_{n+1}) \\ \varphi'(L_{n+1}) \\ \varphi''(L_{n+1}) \\ -\psi(L_{n+1}) \end{bmatrix} = \begin{cases} W_{11}(0) = 0 \\ W'_{11}(0) = 0 \\ W_{1n+1}(L) = 0 \\ W_{1n+1}(L) = 0 \end{cases} \quad (19)$$

$$\begin{bmatrix} \phi_2(L_{n+1}) & \phi_3(L_{n+1}) & \phi_4(L_{n+1}) & \phi_5(L_{n+1}) \\ \varphi'_2(L_{n+1}) & \varphi'_3(L_{n+1}) & \varphi'_4(L_{n+1}) & \varphi'_5(L_{n+1}) \\ \varphi''_2(L_{n+1}) & \varphi''_3(L_{n+1}) & \varphi''_4(L_{n+1}) & \varphi''_5(L_{n+1}) \\ -\psi_{2n}(L_{n+1}) & -\psi_{3n}(L_{n+1}) & -\psi_{4n}(L_{n+1}) & -\psi_{5n}(L_{n+1}) \end{bmatrix}$$

$$K_n = H(L_{n+1} - x_{n+10}) \begin{bmatrix} \phi_{11}(L_{n+1} - x_{n+10}) \\ \varphi'_{11}(L_{n+1} - x_{n+10}) \\ \varphi''_{11}(L_{n+1} - x_{n+10}) \\ -\psi_{1n}(L_{n+1} - x_{n+10}) \end{bmatrix} - H(L_n - x_{n0}) \begin{bmatrix} \phi_{11}(L_n - x_{n0}) \\ \varphi'_{11}(L_n - x_{n0}) \\ -\varphi''_{11}(L_n - x_{n0}) \\ \varphi_{1n}(L_n - x_{n0}) \end{bmatrix} \quad (16)$$

式中

$$\left. \begin{aligned} \phi_m &= \varphi'_m - \frac{1}{R} \bar{\varphi}_m \\ \bar{\psi}_{mi} &= -J_i EI \phi'_m + \phi_m \\ \psi_{mn} &= J_n EI \phi'_m + \phi_m \\ (m &= 1, 2, \dots, 5; i = 1, 2, \dots, n-1) \end{aligned} \right\} \quad (17)$$

根据传递方程式 (14a) 和式 (14b) 建立未知常数向量  $U_1$  和  $U_{n+1}$  的关系

$$U_{n+1} = (T_{2n})^{-1} T_{1n} \left[ \prod_{j=1}^{n-1} (T_{2n-j})^{-1} T_{1n-j} \right] U_1 - (T_{2n})^{-1} \left[ \sum_{k=0}^{n-2} \prod_{l=0}^k T_{1n-l} (T_{2n-l-1})^{-1} K_{n-k-1} \right] - (T_{2n})^{-1} K_n \quad (18)$$

考虑到本文采用的是悬臂式压电俘能器, 已知悬臂梁的边界条件是

将边界条件 (19) 带入传递式 (18) 即可求解未知常数向量  $U_1$  和  $U_{n+1}$ , 再通过式 (14a) 和式 (14b) 可以定义其余未知常数向量.

因此, 可以得到所有局部坐标系下的格林函数, 转换坐标后, 含  $n$  个裂纹的曲梁压电俘能器的格林函数为

$$G_1(x, x_0) = \begin{cases} \bar{G}_{11}(x_1; x_{10}), & x \in [0, L_1^-] \\ \bar{G}_{1i} \left( x - \sum_{i=1}^k L_i; x_{i0} \right), & x \in \left( \left( \sum_{i=1}^{k-1} L_i \right)^+, \left( \sum_{i=1}^k L_i \right)^- \right) \\ \bar{G}_{1n+1}(L-x; x_{n+10}), & x \in \left( \left( \sum_{i=1}^n L_i \right)^+, L \right] \end{cases} \quad (20)$$

## 2 损伤力电耦合系统解耦

根据线性系统和格林函数的叠加原理, 建立裂纹曲梁的力学位移与电力学方程之间的解析关系, 含裂纹曲梁压电俘能器的位移  $W(x)$  为

$$W(x) = W_1(x) + W_2(x) + W_3(x) = \int_0^L F(\xi) \left[ \bar{G}_1(x_1; x_{10}) + \dots + \bar{G}_i \left( x - \sum_{i=1}^k L_i; x_{i0} \right) + \bar{G}_{n+1}(L-x; x_{n+10}) \right] \xi d\xi + \int_0^L G_2(x; \xi) [\delta(\xi - x_1) - \delta(\xi - x_2)] d\xi + \int_0^L G_3(x; \xi) [H(\xi - x_1) - H(\xi - x_2)] d\xi \quad (21)$$

假设在基础加速度作用下压电曲梁上的外力  $f(x, t)$  是简谐力, 可将外力<sup>[35]</sup> 写作

$$F(x) = (\mu\Omega^2 - i\Omega c_1) A_0 \quad (22)$$

式中,  $A_0$  是指位移的振幅.

结合文献 [22] 中已知的输出电压和本文求解的多裂纹曲梁压电俘能器的格林函数解析式, 可以得到本模型的输出电压

$$\bar{V} = (\mu\Omega^2 - i\Omega c_1)A_0 \left\{ - \int_{x_1}^{x_2} \left[ \int_0^L \bar{G}_1(x; \xi) d\xi + \dots + \int_0^L \bar{G}_i \left( x - \sum_{i=1}^k L_i; \xi \right) d\xi + \int_0^L \bar{G}_{n+1}(L-x; \xi) d\xi \right]'' dx + HA_1 + HA_2 \right\} \left\{ \frac{i\Omega C_p R_l + 1}{i\beta C_p R_l} + \int_{x_1}^{x_2} [\bar{G}_2''(x; x_2) - \bar{G}_2''(x; x_1)] dx + HA_3 + HA_4 + HA_5 + HA_6 \right\} \quad (23)$$

式中

$$HA_1 = \left( \frac{\mu\Omega^2 - i\Omega c_1}{EA} - \frac{1}{R^2} \right) \int_{x_1}^{x_2} \left[ \int_0^L \bar{G}_1(x; \xi) d\xi + \dots + \int_0^L \bar{G}_i \left( x - \sum_{i=1}^k L_i; \xi \right) d\xi + \int_0^L \bar{G}_{n+1}(L-x; \xi) d\xi \right] dx \quad (24a)$$

$$HA_2 = -\frac{1}{EA} (x_2 - x_1) \quad (24b)$$

$$HA_3 = \frac{\vartheta_2}{EAR} (x_1 - x_2) \quad (24b)$$

$$HA_4 = - \int_{x_1}^{x_2} \left[ \int_0^L \bar{G}_3(x; \xi) d\xi \right]'' dx \quad (24c)$$

$$HA_5 = \left( \frac{1}{R^2} + \frac{i\Omega c_1 - \mu\Omega^2}{EA} \right) \int_{x_1}^{x_2} [\bar{G}_2''(x; x_2) - \bar{G}_2''(x; x_1)] dx \quad (24d)$$

$$HA_6 = \left( \frac{\mu\Omega^2 - i\Omega c_1}{EA} - \frac{1}{R^2} \right) \int_{x_1}^{x_2} \int_0^L \bar{G}_3''(x; \xi) d\xi dx \quad (24e)$$

因此, 压电俘能器的功率为

$$P = \bar{V}^2 / R_l \quad (25)$$

### 3 数值结果与讨论

本文探究了弧长  $L = 0.1 \text{ m}$ , 宽  $b = 0.01 \text{ m}$  受简谐激励的悬臂曲梁压电俘能器, 曲梁由上层的压电层和下层的结构层组合, 其厚度分别为  $0.005 \text{ m}$  和  $0.005 \text{ m}$ . 曲梁几何和材料参数、压电参数取值如表 1 所示. 其次, 从裂纹几何参数 (裂纹深度和位置) 对裂纹压电曲梁进行了模拟, 裂纹深度比  $h'$  分别为  $0.02, 0.04$  和  $0.06$ , 用裂纹位置  $L_1$  表示离固定端的距离. 在以下算例中, 没有考虑阻尼的影响. 为了方便起见, 引入阻尼效应的无量纲化

$$\zeta_1 = \frac{c_1}{2\mu\Omega_0} \quad (26)$$

式中,  $\Omega_0 = \pi^2 \sqrt{EI/\rho A}/L^2$  是曲梁的一阶固有频率.

表 1 裂纹压电曲梁的几何参数和压电参数取值  
Table 1 Geometrical and electromechanical parameters of the cracked beam

Parameters	Value	Parameters	Value
radius, $R/\text{m}$	0.5	resistance load, $R_l/\Omega$	$1.0 \times 10^6$
electrode start distance from the base, $x_1/\text{m}$	0	electrode end distance from the base, $x_2/\text{m}$	0.1
Young's modulus of substructure layer, $E_s/\text{Pa}$	$1.0 \times 10^{11}$	Young's modulus of piezoelectric layer, $E_p/\text{Pa}$	$6.6 \times 10^{10}$
piezoelectric constant, $d_{31}/(\text{m} \cdot \text{V}^{-1})$	$-1.90 \times 10^{10}$	permittivity $\epsilon_{33}/(\text{nF} \cdot \text{m}^{-1})$	15.93

#### 3.1 解的有效性验证

令裂纹深度为零, 含裂纹的曲梁可退化为完整曲梁模型. 利用这一点将含裂纹压电曲梁的解析解与文献 [22] 得到的完整压电曲梁模型的解作对比, 验证结果是否一致. 如图 2 所示, 本文的位移频率响应结果与文献中的结果基本吻合, 从而验证了本文解的有效性.

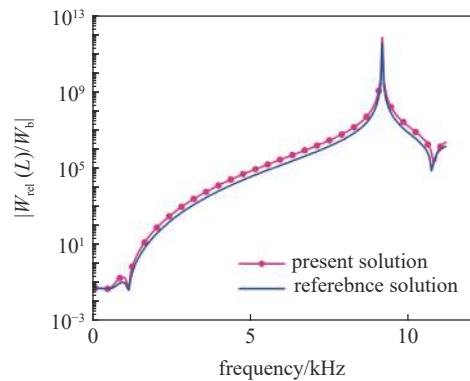


图 2 位移-频率响应的对比图

Fig. 2 The displacement for comparison of present solutions and the solutions from reference

#### 3.2 裂纹损伤对压电俘能器电压-频率响应的影响

本节探究了压电俘能器电压响应在裂纹几何参数影响下的变化. 一方面为相关设计提供了理论依据, 另一方面介绍了如何通过电压响应的变化对结构进行损伤监测.

图 3 绘制了不同裂纹深度时压电俘能器的电压-频率响应图. 从图中可以看出, 频率在到  $5 \text{ kHz}$



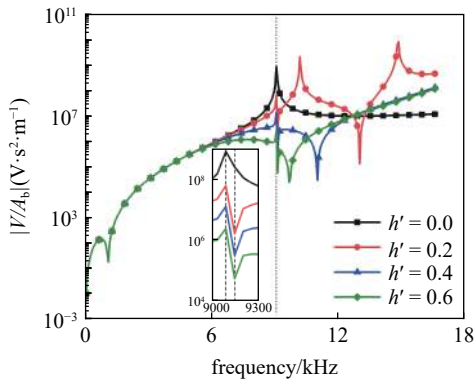


图 3 不同裂纹深度的电压-频率响应 ( $L_1 = 0.06$  m)

Fig. 3 The voltage frequency responses with different crack depths ( $L_1 = 0.06$  m)

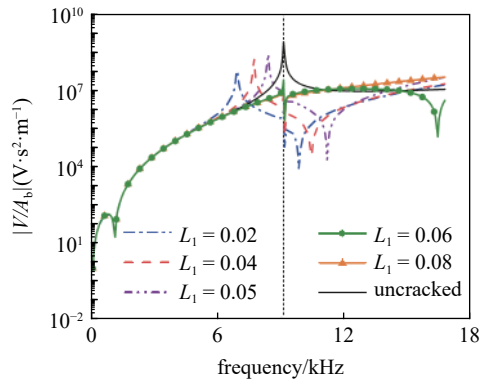
的时候,各裂纹深度的电压响应之间有重叠部分.当振动频率大于此重叠频率振动时,损伤压电曲梁的响应效果与完整曲梁有了显著差异.第一阶频率 9088.6 Hz (虚线处)的峰值随着裂纹深度加深成比例的减小,很快激励出二阶频率 9144.4 Hz,峰值的波动较小并且同样成比例减小.深度加深至 0.7 左右后,一阶频率甚至出现在 9088.6 Hz 之前,且峰值极低.特别说明,此时的二阶频率 9144.4 Hz 时开路条件下压电曲梁的一阶频率值.

对于浅裂纹 ( $0 < h' < 0.2$ ),激励出正向峰值的三阶频率;而在较深裂纹 ( $h' > 0.2$ )的情况下,三阶频率的峰值远远小于浅裂纹时三阶频率的峰值,且随着裂纹加深频率向一阶频率方向偏移.因此,在不同裂纹深度时,压电曲梁的电压响应变化情况的趋势一致的.

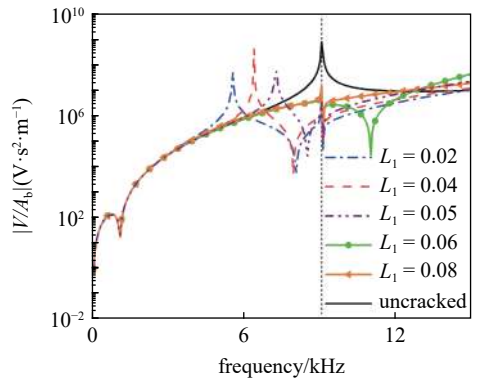
裂纹损伤可能会出现在曲梁结构的任何位置,由图 3 可知,裂纹深度的深浅引起的电压-频率响应变化的差别较大.因此在研究俘能器在裂纹位置变化下的电压响应时,分别考虑了浅裂纹和深裂纹两种情况.

如图 4 所示,随着裂纹位置不断从曲梁固定端靠近曲梁中部,一阶固有频率逐渐增加.但在图 4(a)中,一阶频率的峰值会不断增大,二阶频率 9088.6 Hz 和三阶频率 9144.4 Hz 的峰值变大,且四阶频率也向右偏移.而在图 4(b)中,压电俘能器在 9088.6 Hz 前就被激励出了一阶和二阶频率,且频率皆向右偏移.当裂纹位置从曲梁中部不断靠近曲梁的自由端时,一阶频率和二阶频率仍是 9088.6 Hz 和 9144.4 Hz,且峰值变大,而三阶频率同样发生向右偏移.

总的来说,不同裂纹深度和位置的损伤曲梁压



(a)  $h' = 0.2$



(b)  $h' = 0.4$

图 4 不同裂纹位置下的电压-频率响应

Fig. 4 The voltage frequency responses with different crack locations

电俘能器的电压响应的趋势是一致的,不同的是被激励出的频率以及峰值.

因此想要检测结构的损伤情况,就要根据结构振动响应引起的俘能器的电压响应变化.一旦有裂纹出现,健康曲梁的一阶频率就不再是损伤曲梁的一阶频率,且随着裂纹加深该频率处峰值变小,由此可以判断出出现损伤时裂纹的深度情况.如若损伤曲梁被激励出了一阶频率小于健康曲梁的频率,说明曲梁的固定端到中部这一段结构中出现了裂纹,此时的裂纹深度也可以根据损伤曲梁是否在健康曲梁的一阶频率值前出现反向峰值的二阶频率.相反,如若损伤曲梁被激励出了一阶频率等于健康曲梁的一阶频率,则损伤出现的范围在曲梁的中部至自由端.至此,本文提出的根据结构振动引起的压电俘能器信号响应变化监测结构损伤的逆方法得以验证.

从上述裂纹几何参数对压电俘能器电压响应的分析中可以看出,在很多情况下固有频率都会发生偏移.因此,利用固有频率是否发生偏移这一条件仅能够监测结构中是否有损伤产生,并不能准确检测出结构的损伤情况.

### 3.3 阻尼比对损伤压电曲梁电压-频率响应的影响

考虑到结构中阻尼的影响不可忽视, 研究了电压与阻尼之间的关系, 以预测在有阻尼的压电曲梁发生裂纹损伤时可能出现的情况. 从图 5 中可以看出随着阻尼增大, 电压响应如预期般减小. 在阻尼比取值到 0.8 时, 共振峰基本消失, 响应曲线趋于平缓. 并且几乎在所有情况下, 引入阻尼都会降低电压.

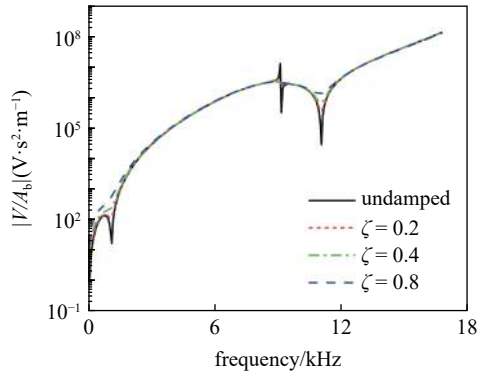


图 5 不同阻尼比下的电压-频率响应 ( $L_1 = 0.04$  m,  $h' = 0.4$ )

Fig. 5 The voltage frequency responses with different damping coefficients ( $L_1 = 0.04$  m,  $h' = 0.4$ )

### 3.4 功率对损伤压电曲梁电压-频率响应的影响

图 6 绘制了不同裂纹深度下压电曲梁的输出功率的频率响应. 可以看出功率响应的变化情况与图 3 电压响应变化相同, 在一阶、二阶频率处的峰值也是成比例减小.

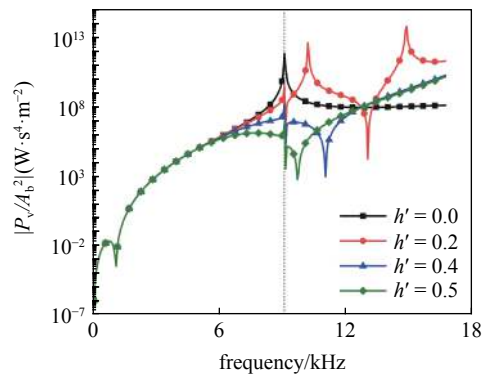


图 6 不同裂纹深度下的功率-频率响应 ( $L_1 = 0.06$  m)

Fig. 6 The frequency responses of electric power with difference crack depth ( $L_1 = 0.06$  m)

## 4 结论

本文重点研究了裂纹损伤的曲梁压电俘能器的力电耦合强迫振动, 运用格林函数法推导出该振动问题的解析解. 在数值计算中, 通过与健康压电曲梁的文献解进行对比, 验证了解的有效性. 最后通过研

究曲梁压电俘能器在裂纹几何参数影响下电压响应变化情况对结构进行损伤监测, 得出结论:

(1) 裂纹出现时, 损伤曲梁的电压响应在健康曲梁的一阶频率处成比例变小, 且随即被激励出二阶频率;

(2) 通过对电压响应的监测可以确定的损伤裂纹的深度和在结构中出现的范围, 证明了逆方法的可行性;

(3) 通过监测由振动响应引起的俘能器电压变化能准确地反映结构的健康状况.

## 参 考 文 献

- 张博, 潘孟春, 胡佳飞等. 微压电梁振动一体化测试方法. 传感器与微系统, 2020, 39(9): 122-125 (Zhang Bo, Pan Mengchun, Hu Jiafei, et al. Micro piezoelectric beam vibration integration test method. *Transducer and Microsystem Technologies*, 2020, 39(9): 122-125 (in Chinese))
- 蔡斌, 周立明. 基于非均匀光滑有限元法的功能梯度压电梁自由振动分析. 中南大学学报 (自然科学版), 2016, 47(1): 48-53 (Cai Bin, Zhou Liming. Inhomogeneous smoothed finite element for free vibration analysis of functionally gradient piezoelectric cantilevers. *Journal of Central South University (Science and Technology)*, 2016, 47(1): 48-53 (in Chinese))
- 刘琪才, 何渊, 王德波. 悬臂梁压电式能量收集器频带扩展研究. 微电子学, 2021, 51(2): 255-259 (Liu Qicai, He Qi, Wang Debo. Research on frequency band extension of cantilever beam piezoelectric energy harvester. *Microelectronics*, 2021, 51(2): 255-259 (in Chinese))
- 李中翔, 胡纯, 郑德智等. 基于压电效应的激光测振仪校准理论方法研究. 传感技术学报, 2020, 33(8): 1122-1126 (Li Zhongxiang, Hu Dun, Zheng Dezhi, et al. Research on calibration theory of laser vibrometer based on piezoelectric effect. *Chinese Journal of Sensors and Actuators*, 2020, 33(8): 1122-1126 (in Chinese))
- Amini Y, Heshmati M, Fatehi P, et al. Piezoelectric energy harvesting from vibrations of a beam subjected to multi-moving loads. *Applied Mathematical Modelling*, 2017, 49: 1-16
- Duan WH, Quek ST, Wang Q. Free vibration analysis of piezoelectric coupled thin and thick annular plate. *Journal of Sound and Vibration*, 2005, 281(1): 119-139
- 周伟建, 陈伟球. 具有表面效应的压电半空间中的表面波. 力学学报, 2017, 49(3): 597-604 (Zhou Jianwei, Chen Weiqiu. Surface waves in a piezoelectric half-space with surface effect. *Chinese Journal of Theoretical and Applied Mechanics*, 2017, 49(3): 597-604 (in Chinese))
- Erturk A, Inman DJ. A distributed parameter electromechanical model for cantilevered piezoelectric energy harvesters. *Journal of Vibration and Acoustics*, 2008, 130(4): 041002
- Erturk A, Inman DJ. On mechanical modeling of cantilevered piezoelectric vibration energy harvesters. *Journal of Intelligent Material Systems and Structures*, 2008, 19(11): 1311-1325
- Zhao X, Yang EC, Li YH, et al. Closed-form solutions for forced vibrations of piezoelectric energy harvesters by means of Green's func-

- tions. *Journal of Intelligent Material Systems and Structures*, 2017, 28(17): 2372-2387
- 11 Zhou SX, Lei Z. Nonlinear dynamic analysis of asymmetric tristable energy harvesters for enhanced energy harvesting. *Communications in Nonlinear Science and Numerical Simulation*, 2018, 61: 271-284
- 12 Huang DM, Chen JY, Zhou SX, et al. Response regimes of nonlinear energy harvesters with a resistor-inductor resonant circuit by complexification-averaging method. *Science China Technological Sciences*, 2021, 64(6): 1212-1227
- 13 Fang ST, Wang S, Miao G, et al. Comprehensive theoretical and experimental investigation of the rotational impact energy harvester with the centrifugal softening effect. *Nonlinear Dynamics*, 2020, 101(1): 123-152
- 14 刘祥建, 陈仁文. Rainbow 型压电换能结构的有限元分析与实验. *光学精密工程*, 2011, 19(4): 789-796 (Liu Xiangjian, Chen Renwen. Finite element analysis and experiments on rainbow shape piezoelectric energy transferring elements. *Optics and Precision Engineering*, 2011, 19(4): 789-796 (in Chinese))
- 15 Luo QT, Tong LY. Design and testing for shape control of piezoelectric structures using topology optimization. *Engineering Structures*, 2015, 97: 90-104
- 16 王剑, 赵国忠, 王悦东等. 压电曲梁单元及其形状控制. *计算力学学报*, 2011, 28(4): 641-646 (Wang Jian, Zhao Guozhong, Wang Yuedong, et al. Shape control of piezoelectric structures by curved beam actuators. *Chinese Journal of Computational Mechanics*, 2011, 28(4): 641-646 (in Chinese))
- 17 周勇, 李荣华, 李实等. 压电层合曲梁大变形的精确分析. *压电与声光*, 2016, 38(1): 88-93 (Zhou Yong, Li Ronghua, Li Shi, et al. Precise analysis of the finite deformation of curved beams covered with PZT actuators. *Piezoelectrics & Acousto-optics*, 2016, 38(1): 88-93 (in Chinese))
- 18 丁维高, 谢进. 压电曲梁俘能器的机电耦合方程及其研究. *压电与声光*, 2018, 40(5): 684-689 (Ding Weigao, Xie Jin. Study on the electromechanical coupling equations of piezoelectric curved beam harvester. *Piezoelectrics & Acousto-optics*, 2018, 40(5): 684-689 (in Chinese))
- 19 Kathpalia B, Tan D, Stern I, et al. Modeling and characterization of a curved piezoelectric energy harvester for smart paver tiles. *Procedia Computer Science*, 2017, 109: 1060-1066
- 20 Chen MF, Chen HL, Ma XL, et al. The isogeometric free vibration and transient response of functionally graded piezoelectric curved beam with elastic restraints. *Results in Physics*, 2018, 11: 712-725
- 21 Tabatabaei-Nejhad SZ, Malekzadeh P, Eghtesad M. Out-of-plane vibration of laminated FG-GPLRC curved beams with piezoelectric layers. *Thin-Walled Structures*, 2020, 150: 106678
- 22 何燕丽, 赵翔. 曲梁压电俘能器强迫振动的格林函数解. *力学学报*, 2019, 51(4): 1170-1179 (He Yanli, Zhao Xiang. Closed-form solutions for force vibration of curved piezoelectric energy harvesters by means of Green's function. *Chinese Journal of Theoretical and Applied Mechanics*, 2019, 51(4): 1170-1179 (in Chinese))
- 23 王永亮. 含裂纹损伤圆弧曲梁弹性屈曲的有限元网格自适应分析. *工程力学*, 2021, 38(2): 8-15 (Wang Yongliang. Adaptive mesh refinement analysis of finite element method for elastic buckling of cracked circularly curved beams. *Engineering Mechanics*, 2021, 38(2): 8-15 (in Chinese))
- 24 Khiem, NT, Lien TV. The dynamic stiffness matrix method in forced vibration analysis of multiple-cracked beam. *Journal of Sound and Vibration*, 2002, 254(3): 541-555
- 25 Caddemi S, Caliò I. Exact closed-form solution for the vibration modes of the Euler-Bernoulli beam with multiple open cracks. *Journal of Sound and Vibration*, 2009, 327(3-5): 473-489
- 26 Nicoletti R. On the natural frequencies of simply supported beams curved in mode shapes. *Journal of Sound and Vibration*, 2020, 485: 115597
- 27 刘刚, 黄一, 陈景杰等. 基于 PVDF 的拉伸状态下平板结构表面裂纹损伤检测实验研究. *机械强度*, 2008, 30(5): 848-853 (Liu Gang, Huang Yi, Chen Jingjie, et al. Experimental study on surface crack detection of plate structures under tension using PVDF films. *Journal of Mechanical Strength*, 2008, 30(5): 848-853 (in Chinese))
- 28 张敬芬, 赵德有. 工程结构裂纹损伤振动诊断的发展现状和展望. *振动与冲击*, 2002, 21(4): 22-26 (Zhang Jingfen, Zhao Youde. Summary review of vibration-based crack diagnosis technique for engineering structures. *Journal of Vibration and Shock*, 2002, 21(4): 22-26 (in Chinese))
- 29 孙威, 阎石, 焦莉等. 基于压电波动法的混凝土裂缝损伤监测技术. *工程力学*, 2013, 30(B06): 206-211 (Sun Wei, Yan Shi, Jiao Li, et al. Monitoring technology for crack damage of concrete structure based on piezoelectric wave method. *Engineering Mechanics*, 2013, 30(B06): 206-211 (in Chinese))
- 30 Hou S, Zhang HE, Ou JQ. A PZT-based smart aggregate for seismic shear stress monitoring. *Smart Materials and Structures*, 2013, 22(6): 065012
- 31 Markovic N, Nestorovic T, Stojic D. Numerical modeling of damage detection in concrete beams using piezoelectric patches. *Mechanics Research Communications*, 2015, 64: 15-22
- 32 Fernández-Sáez J, Rubio L, Navarro C. Approximate calculation of the fundamental frequency for bending vibrations of cracked beams. *Journal of Sound and Vibration*, 1999, 225: 345-352
- 33 Zhao X, Zhao YR, Gao XZ et al. Green's functions for the forced vibrations of cracked Euler-Bernoulli beams. *Mechanical Systems and Signal Processing*, 2016, 68-69: 155-175
- 34 Karaagac C, Ozturk H, Sabuncu M. Crack effects on the in-plane static and dynamic stabilities of a curved beam with an edge crack. *Journal of Sound and Vibration*, 2011, 330(8): 1718-1736
- 35 Danesh-Yazdi AH, Elvin N, Andreopoulos Y. Green's function method for piezoelectric energy harvesting beams. *Journal of Sound and Vibration*, 2014, 333(14): 3092-3093